Design and experimental study of superconducting left-handed transmission lines with tunable dispersion

Design and experimental study of superconducting left-handed transmission lines with tunable dispersion

E A Ovchinnikova[1], S Butz[2], P Jung[2], V P Koshelets[1,3], L V Filippenko[1,3], A S Averkin[1], S V Shitov[1,3] and A V Ustinov[1,2]

[1] National University of Science and Technology (MISIS), Leninsky prospekt 4, Moscow 119049, Russia
[2] Physikalisches Institut, Karlsruhe Institute of Technology (KIT), D-76131 Karlsruhe, Germany
[3] Kotel'nikov Institute of Radio Engineering and Electronics, Moscow 125009, Russia

E-mail: elhed@yandex.ru (E A Ovchinnikova)

Abstract
We study the microwave properties of a superconducting tunable coplanar waveguide (CPW). Pairs of Josephson junctions are forming superconducting quantum interference devices (SQUIDs), which shunt the central conductor of the CPW. The Josephson inductance of the SQUIDs is varied in the range of 0.08–0.5 nH by applying a dc magnetic field. The central conductor of the CPW contains Josephson junctions connected in series that provide extra inductances; the magnetic field controlling the SQUIDs is weak enough not to influence the inductance of the chain of the single junctions. The circuit is designed to have left- and right-handed transmission properties separated by a variable rejection band; the band edges can be tuned by the magnetic field. We present transmission measurements on CPWs based on up to 120 Nb–AlO$_x$–Nb Josephson junctions. At zero magnetic field, we observed no rejection band in the frequency range of 8–11 GHz. When applying the magnetic field, a rejection band between 7 GHz and 9 GHz appears. The experimental data are compared with numerical simulations.

(Some figures may appear in colour only in the online journal)

1. Introduction

Left-handed electromagnetic materials were considered in 1967 by Veselago [1]. Using Maxwell equations, it was shown that such materials exhibit a negative index of refraction. The medium was called 'left' or 'left-handed' (LH) because the electric field E, magnetic field H and the wavevector k form a left-handed system, while in ordinary media they form a right-handed system. According to the Maxwell equations, the phase velocity of the LH media is opposite to both the direction of energy flow and the group velocity [2]. Since their first experimental realization in 2000 [3], the interest in left-handed metamaterials is unbroken and growing. One relatively simple way of implementing a left-handed medium is the building of a planar transmission line. The electric permittivity ε and magnetic permeability μ of such

a transmission medium can be modeled using distributed L–C networks [4]. The traditional two-wire model of a right-handed transmission line (RHTL) with inductance L on the central conductor and capacitance C on the shunt describes an electromagnetic medium with a positive index of refraction, where L and C define positive equivalents for permeability and permittivity, respectively. A left-handed transmission line (LHTL) with negative permeability and permittivity can be created by simply exchanging the positions of L and C in the line [5].

2. Design and computer simulation

A transmission line can be described by the purely left-handed or right-handed two-wire model. However, in reality, it will always be of mixed type while LHTL or RHTL behavior can

dominate within a fixed frequency range [6]. In this work, we propose, design and test a transmission line which is tunable from RHTL to LHTL under application of a dc magnetic field. The tunability of LHTLs has already been considered in some work, for example in [7, 8]. In [7], the pass-band of the line is changed by applying a dc bias current, which tunes the kinetic inductance of a superconducting wire. The tunability has been also provided via applying a static electric field to thick films of barium–strontium–titanate (BST) which changes the electrical properties of the structure.

The suggested transmission line contains dc SQUIDs as tunable elements, which are known for their high sensitivity to magnetic fields. The tuning of the dispersion is obtained by changing the Josephson inductance of the SQUIDs. Previously, Josephson junction arrays with two-junction unit cells have been studied theoretically in [9]. Here, we focus on the experimental study of a tunable rejection band in the transmission spectrum of the planar CPW. Our approach relies on the tunability of SQUIDs, which has been recently experimentally demonstrated in [10].

The Josephson inductance of the dc SQUID is given by the relation from [11]:

$$L_j = \frac{\Phi_0}{2\pi I_c \cos \varphi},$$
(1)

where Φ_0 is the magnetic flux quantum, I_c is the maximum (zero field) critical current of the junction and φ is the superconducting phase difference. The phase difference defines the superconducting current through the junction in a non-zero magnetic field. It is essential to notice that the influence of the magnetic field on the inductance L_{j1} of the series of Josephson junctions in the main line is negligible because the applied magnetic field is normal to the plane of the electrodes of the junction. The magnetic flux coupled to the series junctions is negligibly small, therefore the inductance L_{j1} of the junctions can be assumed as a constant for the whole range of magnetic fields used in this experiment.

The lumped-element equivalent circuit of a section of our transmission line is shown in figure 1. Capacitance C_1 and inductance L_{j2} define the left-handed properties of the transmission line while capacitance C_2 and inductance L_{j1} contribute to the right-handed behavior. Since both chains C_1–L_{j1} and C_2–L_{j2} are resonators, one would expect that the line may have, depending on exact parameters of C' and L', properties of either type in different frequency bands.

In order to understand the LHTR properties, one has to consider the dispersion relation $f(\beta)$ of traveling waves as in [7]. The propagation constant β shows the phase and amplitude of electromagnetic wave along the propagation direction. An example of the frequency dependence of the propagation constant β is shown in figure 2 which is calculated for the following parameters specific to our circuit: $C_1 = 2.1$ pF, $C_2 = 1.7$ pF, $L_{j1} = 80$ pH. The tunable inductance L_{j2} is controlled by a small uniform dc magnetic field, which induces dissipation-free persistent currents in the loops of the SQUIDs. Figure 2(a) shows an example of the dispersion curve for $L_{j2} = 300$ pH, while in figure 2(b) we use $L_{j2} = 190$ pH.
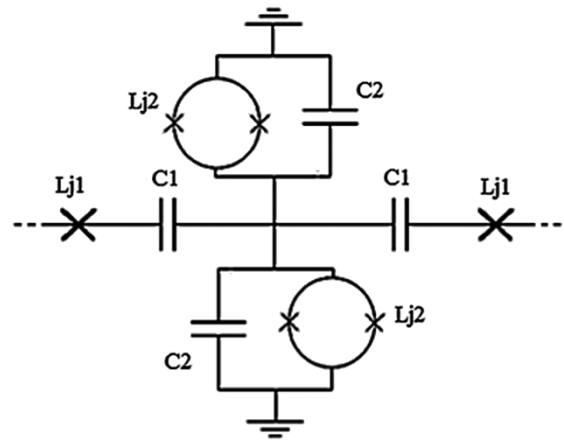

Figure 1. Scheme of a unit cell. Crosses indicate Josephson junctions, circles are SQUID loops and L_j denote the effective inductance of either SQUIDs or Josephson junctions. The experimental devices contains up to 20 cells in series, which is long enough to treat the structure as a fraction of a transmission line within the frequency range 4–12 GHz.

One can see from figure 2 that the phase and group velocities, V_{Ph} and V_g, have opposite signs in the lower part of the dispersion spectrum. This mean that the lower transmission band is the left-handed band. In contrast, phase and group velocities have the same direction above the upper cut-off frequency, which indicates a right-handed band. The lower and upper cut-off frequencies shown in the text below are respectively the upper frequency of the left-handed band and the lower frequency of the right-handed band. These cut-off frequencies can be expressed via the following equations from [12]:

$$f_{c1} = \frac{1}{2\pi\sqrt{L_{j1}C_1}}; \qquad f_{c2} = \frac{1}{2\pi\sqrt{\frac{1}{2}L_{j2}C_2}}.$$
(2)

It can be seen from equations (1) and (2) that changing L_{j2} one can tune the upper frequency of the rejection band.

We started our study with numerical simulation of the transmission through an array of 20 unit cells from figure 1. The results of the simulation are shown in figure 3 for different values of φ, corresponding to different values of the magnetic field. One can see that the dip in the transmission between the left-handed (lower band) and the right-handed (higher band) indeed depends on the inductance L_{j2}, which is controlled via application of magnetic field, as expected from equations (1) and (2). In figure 3(a) only one, the left-handed pass-band, is present. The application of magnetic field leads to the merging of the left and right-handed pass-bands as shown in figure 3(b). At even larger field $\cos \varphi$ gets close enough to zero, and the left-handed and right-handed bands of transmission are again separated by a rejection band. This case is depicted in figure 3(c).

The transmission from figure 3 does not indicate the left-handed and right-handed behavior directly. The scattering parameters (*S*-parameters) and the complex impedance of the cells can be used to clarify whether the band is left-handed or right-handed. Both *S*-parameters and impedance for the
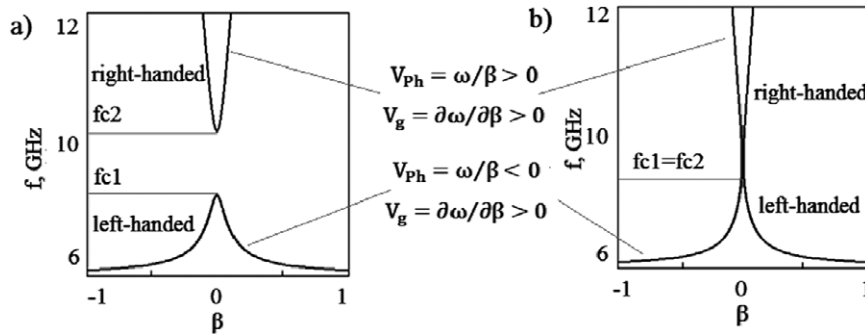
Figure 2. Calculated dispersion curves of LHTL. (a) Josephson inductance $L_{j2} = 300$ pH leads to $f_{c1} \neq f_{c2}$; a rejection band occurs between frequencies f_{c1} and f_{c2}. (b) Josephson inductance $L_{j2} = 190$ pH results in $f_{c1} = f_{c2}$; the rejection band is absent.
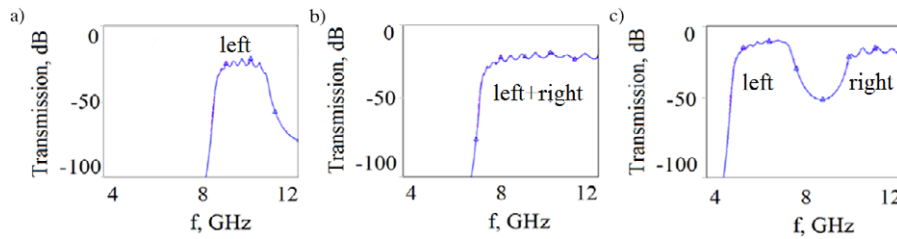

Figure 3. Simulated transmission magnitude $|S_{21}|$ through an array of 20 unit cells for different values of φ: (a) $\cos \varphi = 0.8$, (b) $\cos \varphi = 0.4$, (c) $\cos \varphi = 0.2$.
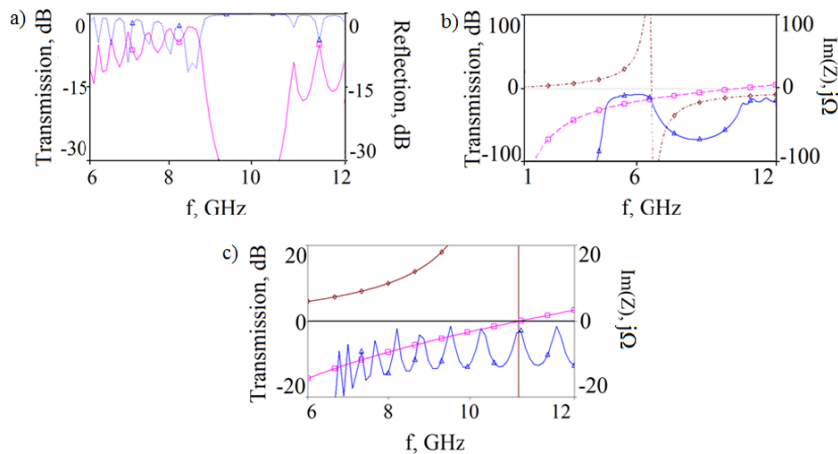

Figure 4. (a) Simulated scattering parameters $|S_{11}|$ (blue, right axis) and $|S_{21}|$ (magenta, left axis) for 20 unit cells. (b) Transmission through 20 unit cells (blue, left axis) and impedance of serial (magenta, right axis) and parallel (blue, right axis) elements for $\cos \varphi = 0.2$ and $f_{c1} \neq f_{c2}$. (c) Transmission through 20 unit cells (blue, left axis) and impedance of serial (magenta, right axis) and parallel (brown, right axis) elements for $\cos \varphi = 0.4$ and $f_{c1} = f_{c2}$.

magnetic fields of figure 3(c) are depicted in figure 4. One can see from figure 4(a) that the structure demonstrates almost full reflection ($S_{11} = 0$ dB) within the frequency range of 9–11 GHz. According to figure 4(b), the edges of the reflection band coincide with the frequencies at which the imaginary part of the impedance curves, Im(Z, f), change their sign. The left-handed behavior, by definition of the model, corresponds to the reactive impedance of the parallel elements Im$(Z_{\text{shunt}}) > 0$ (inductor) and, simultaneously, the reactive impedance of the series elements Im$(Z_{\text{series}}) < 0$ (capacitor), while the right-handed behavior occurs for opposite signs of these impedances. In figure 4(c), one can

see the impedance of serial and parallel elements, which corresponds to the bands shown in figure 3(b). In this case, $f_{c1} = f_{c2}$ and the change of signs of the imaginary parts of the impedance appears at the same frequency. Since there is no band where the impedances are simultaneously both negative and positive, no rejection gap exists between the right- and left-handed frequency bands, as figure 2(b) shows. Note, however, that the absolute value of the transmission is far from 100% even within the transmission bands. This is due to the impedance mismatch between the characteristic impedance of the line and the standard ports of 50 Ω considered in the simulation.
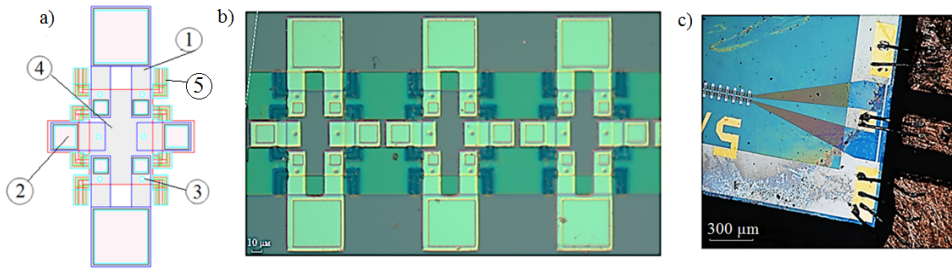
Figure 5. Experimental sample close-up. (a) Cell layout: 1—SQUID loop with large capacitor to ground, 2—via bridge connecting neighboring cells, 3—one of six Josephson junctions of the cell, 4—the bottom electrode is the central island of the cell. (b) Optical microscope image of three cells of the LHTL. (c) Optical microscope image of the connection to the 50-Ω CPW.
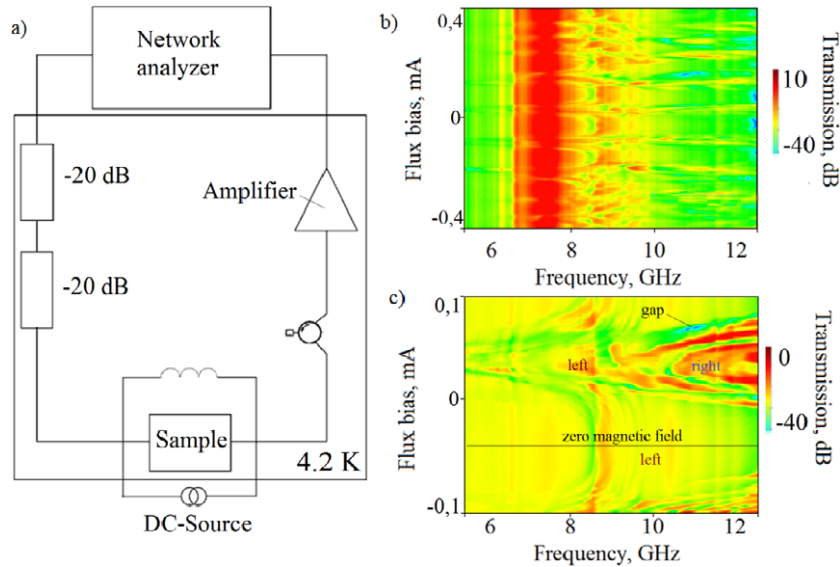

Figure 6. (a) Scheme of the experimental setup. (b) Measured transmission through the transmission line containing 10 cells as function of magnetic field. The magnetic field ranges from −0.4 to 1 mT. No virtual calibration is used. (c) Measured transmission with subtracted background (virtual calibration) for 20-cell line as function of magnetic field. The magnetic field range is between −0.2 and 0.6 mT.

3. Experiment

A number of features of the experimental layout have to be restricted to the resolution of the fabrication process of the Josephson junctions. Fortunately, the trilayer process Nb–AlO$_x$–Nb available to us ensures sufficient compactness of the unit cell. This process makes it possible for us to use parallel plate capacitors formed by two niobium layers and an insulation layer from anodic oxide Nb$_2$O$_5$ for all capacitors. Note that the SQUIDs are operating in the superconducting state, and no resistive shunts are used. The layout of the cell, an optical image of the three experimental cells and the wiring at the sample holder are illustrated in figures 5(a)–(c). All six Josephson junctions of each unit cell, which are shown in figure 5(a), are fabricated on a common island. The areas denoted by 5 in figure 5(a) and in dark blue in figure 5(b) are spots where the anodization wiring is etched away at the final stage of the fabrication process. A chip of the size 4 × 4 mm^2 contains two completely separated rf transmission lines (i.e. two samples). The two lines are different: one contains 10 and the other contains 20 unit cells per line. The experimental setup is shown in figure 6(a). The samples are measured using

an Agilent PNA-X network analyzer in a dry close-cycle cryostat at temperatures about 2 K. Additional attenuators (40 dB) are inserted into the input line in order to reduce the external noise and make sure that the probe rf current does not exceed the critical current of the Josephson junctions. Due to the low probe current, it was necessary to boost the output signal by using a low-noise amplifier (LNA). The magnetic field was applied by a superconducting coil external to the sample holder; the field magnitude is proportional to the current through the coil which is shown in the vertical axis of the following plots.

Microwave calibration is not an easy task for cryogenic measurements, as detailed in [13]. Depending on the experimental setup, a proper calibration might not be possible. This is why in this work a virtual calibration for the transmitted signal is attempted. To do this, we averaged the response $S_{21}(f, H)$ for each frequency point, f, over the whole set of data for magnetic field, H, and subtracted the resulting relation $S_{21}^{av}(f)$ from the measured data. This procedure is feasible since we are interested in detecting the variations caused by the magnetic field at a given frequency, not in frequency variation for a static magnetic field. Since we
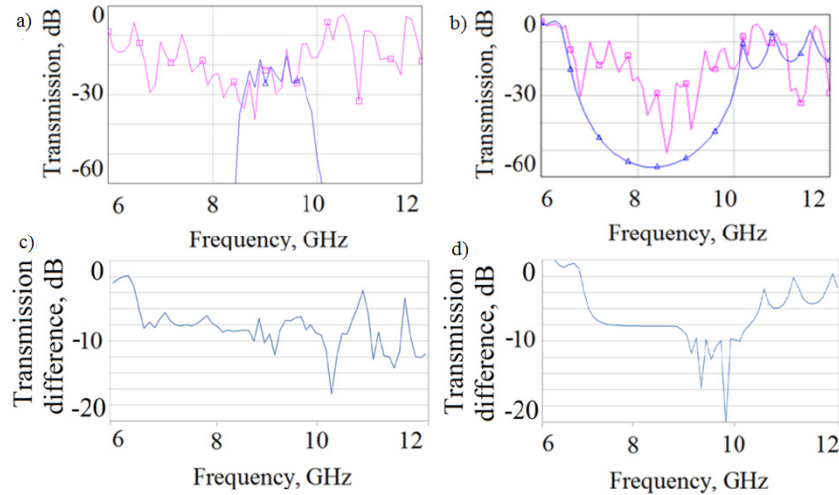
Figure 7. (a) Simulated transmission through the line containing 20 unit cells in the presence of the non-ideal (rf-leaky) sample holder (magenta) and simulation for an ideal (no-leak) sample holder (blue) for a value of $\cos\varphi = 0.8$. (b) Same data and color coding as in (a), but with $\cos\varphi = 0.2$. (c) Expected response to magnetic field (from $\cos\varphi = 0.2$ to 0.8) for the leaky holder as the difference between in transmission (a) and (b). (d) The same difference as in (c) but with an ideal sample holder.

assume that the relative weight of the large deviation of S caused by H is small, the averaged response $S_{21}^{av}(f)$ should deviate slightly from the 'true background'. The transmission through the superconducting LHTL with 10 cells is shown in figure 6(b). No virtual calibration was used here.

One can see from figure 6(b) that the transmission through the line with 10 cells changes periodically with the magnetic field, as expected due to flux quantization. In figure 6(c), we show the transmission with subtracted background $S_{21}^{av}(f)$ for the line with 20 cells. Here, periodic changes of the transmission with the magnetic field are also observed. At zero field ($\varphi = 0$), only one transmission band is seen below 12 GHz. At larger fields $\cos\varphi$ is close enough to zero, and two pass-bands divided by a gap can be seen, as predicted by simulations.

We also observed some discrepancies between simulation and experiment. First, there is moderate transmission below 8 GHz, whereas the simulation predicts negligible transmission (the rejection dip). Second, the frequency range of the rejection band is narrower than predicted. Both these issues can be assigned to a parasitic stray transmission through the sample holder. We simulated this parasitic transmission, which is depicted in figure 7 by the pink curve. The measured rf leak is consistent with the level estimated from the detailed electromagnetic simulations of our sample holder. One can see from figure 7(a) that it is hard to unambiguously extract the cut-off frequency from the experimental data at zero field, not to mention the rejection band limits at relatively large magnetic fields. The unwanted transmission through the holder appears due to, at least, two factors: (i) the holder creates an additional path for the signal, and (ii) the characteristic impedance of the line is strongly mismatched with the 50 Ω input–output lines, as already mentioned. Both these features lead to significant enhancement of the unwanted, but unavoidable rf background and large standing waves in the transmission spectrum as presented in figures 7(a) and (b). To clarify the effect of the rejection

gap we subtracted transmission in smaller magnetic field ($\cos\varphi = 0.8$) from the transmission with larger magnetic field for two cases: (i) with the leaky model of the sample holder (in figure 7(c)) and (ii) with ideal (no-leak) sample holder (in figure 7(d)). From these data one can see that these differential signals are expected to be narrow-band in spite of the fact that the wide-band feature is predicted for an ideal sample holder. The differential signal is predicted to have few dips between the left- and right-handed bands, i.e. between approximately 7 and 11 GHz as presented in figures 7(c) and (d). In this frequency range the transmission is lower in larger magnetic fields than in smaller ones. For both the leaky and the ideal holders the effect is qualitatively the same. This behavior provides a strong indication of the possibility of detecting the predicted gap even with the non-ideal sample holder. The experimental data demonstrate a number of narrow dips as depicted in figure 8. Our virtual calibration via averaging is rather qualitative, so we did not succeed in complete removal of the effect of standing waves in figure 8. Since the impedance of the line changes, the reflected signal (standing wave) also changes with the magnetic field. Nevertheless, the predicted narrow gap is clearly observable: when increasing the magnetic field, it moves to lower frequency and finally disappears, thus merging the left and right-handed bands. Further increase of the magnetic field leads to a reappearance of the gap and makes it deeper again as presented in figure 8. In spite of having observed the rather narrow band gap, this result is supported by the predicted performance as from figures 7(c) and (d).

4. Conclusion

The concept of a superconducting magnetic field tunable left-handed transmission line with Josephson junctions has passed experimental verification within the frequency range of 6–12 GHz. The calculated dispersion of the line shows
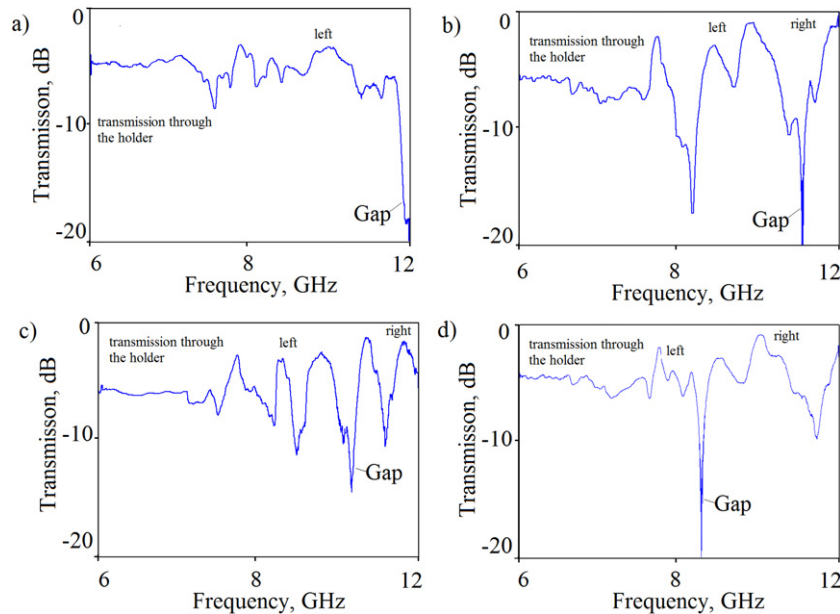
Figure 8. Measured transmission through 20-cell line for various magnetic fields: (a) 0 mT, (b) 0.15 mT, (c) 0.25 mT, and (d) 0.3 mT.

left-handed behavior within the lower frequency transmission band. Experimental data demonstrate the tunability of both the transmission and rejection bands by applying a dc magnetic field. The magnetic field allows us to shift the rejection band between the left- and right-handed transmission. Moreover, for a limited frequency range near 10 GHz, the transmission line can be transformed from left-handed to right-handed by changing the magnetic field. The presented experiments are noticeably obscured by parasitic transmission through the sample holder. An improved design of the sample holder is currently under development and we expect to obtain more detailed data in the near future. The potential for improvement may be found in the design of a better impedance match between the sample and the standard 50-Ω cables.

Acknowledgments

References

[1] Veselago V G 1967 The electrodynamics of substances with simultaneously negative values of ε and μ *Usp. Fiz. Nauk* **92** 517–26

[2] Shen J Q 2008 Introduction to the theory of left-handed media arXiv:cond-mat/0402213

[3] Pendry J and Smith D 2004 Reversing light with negative refraction *Phys. Today* **57** (6) 37–43

[4] Caloz C and Itoh C T 2003 Novel microwave devices and structures based on the transmission line approach of meta-materials *IEEE MTT-S Int. MTT Symp. Dig.* **1** 195–8

[5] Eleftheriades V, Klyer A and Kremer P 2002 Planar negative refractive index media using periodically L–C loaded transmission lines *IEEE Trans. Microw. Theory Tech.* **50** 2702–12

[6] Wang Y and Lancaster J 2006 High-temperature superconducting coplanar left-handed transmission lines and resonators *IEEE Trans. Appl. Supercond.* **16** 1893

[7] Salehi H, Majedi A and Mansour R 2005 Analysis and design of superconducting left-handed transmission lines *IEEE Trans. Appl. Supercond.* **15** 996–9

[8] Durán-Sindreu M, Damm Ch, Sazegar M, Zheng Yu, Bonache J, Jakoby R and Martín F 2011 Electrically tunable composite right/left handed transmission-line based on open resonators and barium–strontium–titanate thick films *Microwave Symp. Digest (MTT), IEEE MTT-S Int.* 1–4

[9] Hutter C, Tholen E A, Stannigel K, Lidmar J and Haviland D B 2011 Josephson junction transmission lines as tunable artificial crystals *Phys. Rev.* B **83** 014511

[10] Jung P, Butz S, Shitov S V and Ustinov A V 2013 Low-loss tunable metamaterials using superconducting circuits with Josephson junctions *Appl. Phys. Lett.* **102** 062601

[11] Schmidt V V 1997 *The Physics of Superconductors* ed P Mueller and A V Ustinov (Berlin: Springer)

[12] Pozar D 1998 *Microwave Engineering* 2nd edn (Toronto: Wiley) pp 424–7, 162

[13] Anlage S M and Yeh J-H 2013 *In situ* broadband cryogenic calibration for two-port superconducting microwave resonators *Rev. Sci. Instrum.* **84** 034706